

# THERMODYNAMIC ANALYSIS OF THE SUPERCRITICAL STARTUP OF CRYOGENIC HEAT PIPES

## Paulo Couto

Federal University of Rio de Janeiro - Department of Mechanical Engineering - EE/COPPE, Cid. Universitária, Cx. Postal 68503  
Rio de Janeiro, RJ, 21945-970, Brazil  
pcouto@littc.coppe.ufrj.br

## Jay M. Ochterbeck

Clemson University - Department of Mechanical Engineering, 221 Fluor Daniel Bldg.  
Clemson, South Carolina, 29634-0921, USA  
jochter@ces.clemson.edu

## Marcia B. H. Mantelli

Federal University of Santa Catarina - Department of Mechanical Engineering - EMC/UFSC, P.O. Box 476  
Florianopolis, SC, 88040-900, Brazil  
marcia@labsolar.ufsc.br

**Abstract.** *An investigation of the supercritical startup of cryogenic heat pipes with parasitic heat loads is presented here. A transient, one-dimensional model developed for microgravity environment available in the literature is used to obtain the axial temperature distribution along the heat pipe, as well as the vapor pressure and working fluid mass distribution in the wick structure and vapor region. Thermodynamic pressure-specific volume diagrams are used to substantiate the investigation. Theoretical and experimental data for microgravity experiments are presented. The results showed that the parasitic heat load can change significantly the operational temperature of the cryogenic heat pipe and it must be accurately considered during the design stages of this kind of device. Also, the fluid charge plays an important role in the determination of the initial thermodynamic state of the cryogenic heat pipe. An excess of fluid charge may prevent a successful startup due to an increased vapor pressure, while a deficiency may prevent the startup due to lack of working fluid to overcome the effects of the parasitic heat loads.*

**Keywords.** *Cryogenic heat pipes, supercritical startup, thermodynamic analysis.*

## 1. Introduction

In 1996, the Satellite Thermal Control Laboratory of the Federal University of Santa Catarina (LABSOLAR/NCTS - UFSC) began the development of a Passive Cryogenic Radiator in the context of the University Program for Space Development (Uniespaço), funded by the Brazilian Space Agency (AEB). Passive Cryogenic Radiators are used to cool down equipments, such as infrared sensors and Charge Coupled Device (CCD) cameras, to the cryogenic temperature levels required for their optimum operation. But, in the most of the satellite designs, the infrared sensor (or the equipment to be cooled) cannot be placed near the cryogenic radiator. Usually, cryogenic heat pipes are used to transfer the heat from these equipments to the cryogenic radiator (Brandt and Schlitt, 1997; Wright, 1980; Wright and Pence, 1973) or any other heat sink (Brennan *et al.*, 1993 and Rosenfeld *et al.*, 1995). In addition, cryogenic heat pipes are used on the thermal control of focal plans of infrared sensors (Voyer *et al.*, 1997), X-ray telescopes (Abrosimov *et al.*, 1992), cooling of superconducting magnets (Ishigohka *et al.*, 1999), among others. The design and analysis of cryogenic heat pipes is now under investigation at the LABSOLAR/NCTS, in order to develop a complete passive cryogenic thermal control device for the payload of the Brazilian satellites described at the Brazilian Policy for Space Activities (*Agência Espacial Brasileira*, 1996).

Cryogenic technology is advancing rapidly in both space and earth-based applications, and with it comes the need for thermal control devices. Cryogenic heat pipes are one of the many different existing types of devices, and they are highly reliable and efficient heat transfer devices considered for many terrestrial and space applications (Peterson, 1991). This device uses the latent heat of vaporization (condensation and evaporation) of a working fluid to transfer thermal energy over a long distance with a small temperature drop. Cryogenic heat pipes usually operate at temperatures below 200 K (Faghri, 1995) and their operational temperature range from the triple point temperature to the critical temperature of the working fluid, which is relatively narrow for cryogenic fluids (Barron, 1985). Cryogenic heat pipes are often used for the thermal control of infrared detectors onboard earth observation (Brandt and Schlitt, 1997), astronomy and military satellites (Groll *et al.*, 1998). Actually, they have also been used in some terrestrial applications, such as cryosurgeries (Hamilton and Hu, 1993) and superconducting devices (Nakano *et al.*, 1996).

Differently from low and medium temperature heat pipes, cryogenic heat pipes start from a supercritical condition. The entire heat pipe must be cooled below its critical point before nominal operation begins (Peterson and Compagna, 1987). When the vapor pressure inside the heat pipe equals the saturation pressure at a given vapor temperature, liquid condenses (Couto, 2003) and a liquid column develops in the wick structure at the condenser section due to the heat sink. As the temperature of the condenser decreases, more vapor condenses and the liquid column advances towards the evaporator end, driven by the capillary force developed at the wick, and opposed by the wall friction. The cooling effect of the liquid vaporization at the liquid column leading edge cools the dry length of the heat pipe, priming the wick structure until steady state operation (Yan and Ochterbeck, 1999).

Cryogenic working fluids usually exhibit very low values of surface tension and latent heat of vaporization, resulting in low heat transport capacity heat pipes, which are very sensitive to parasitic heat loads (Couto *et al.*, 2002), fluid charge (Röster *et al.*, 1987; Groll *et al.*, 1986) and acceleration fields (Ochterbeck *et al.*, 1995). The parasitic heat loads can change significantly the operational temperature of the cryogenic heat pipe, and may add loads of the order of the maximum transport capability of the heat pipe. In addition, the parasitic heat loads can adversely affect the transient start-up behavior of the system. A little excess of fluid charge may help the startup process as it supplies more liquid to the liquid column, increasing its momentum. In the other hand, an excess of liquid increases the vapor pressure, creating a liquid slug during normal operation that may block part of the condenser, decreasing the heat pipe performance. A deficiency of working fluid is never desirable because it may prevent the heat pipe to prime completely during startup. Acceleration fields, such as those provided by orbital attitude adjustments, reboost and docking maneuvers, can cause the redistribution of liquid within the heat pipe, flooding or drying out the evaporator. Acceleration due to gravitational fields (as in ground tests, for example) improves the startup of cryogenic heat pipes as it spreads the liquid slug (developed due to excess of working fluid during the startup) in the wick structure, increasing the momentum of the liquid column (Brennan *et al.*, 1993).

Although simple, the process presents many details that are not clear. The beginning of the condensation process of the working fluid in the wick structure depends on the thermodynamic state of the fluid, *i.e.*, the temperature and the pressure. It is possible that the supercritical working fluid turns into subcooled liquid before the condensation begins. How the subcooled liquid column would behave? How the gravitational forces affect the supercritical startup? How the parasitic heat loads over the heat pipe wall affect the supercritical startup? What is the limit of parasitic heat loads that the heat pipe can withstand? How does the working fluid charge affect the startup process? In the following sections of this work, the questions above will be addressed.

## 2. Supercritical Startup Model

The supercritical startup of axially grooved and porous sintered metal wick cryogenic heat pipes is considered. The initial temperature of the heat pipe,  $T_0$ , is homogeneous and is above the critical temperature. The boundary condition at the condenser region is a specified time-variable temperature [ $T_c = f(t)$ ]. This boundary condition is consistent with most microgravity experiments in the literature (Brennan *et al.*, 1993; Rosenfeld *et al.*, 1995), which use cryocoolers to provide the required heat rejection at the condenser region. The remaining length of the heat pipe (adiabatic and evaporator regions) is considered to be under the effect of a radiative parasitic heat load. This parasitic heat load is provided by the radiative heat transfer between the heat pipe wall and the spacecraft structure, and heat loads from the space environment (*e.g.*, direct sun irradiation, earth infrared emission and albedo, etc.). Figure 1 shows the schematic of the physical model, as well as the boundary conditions and the coordinate system.

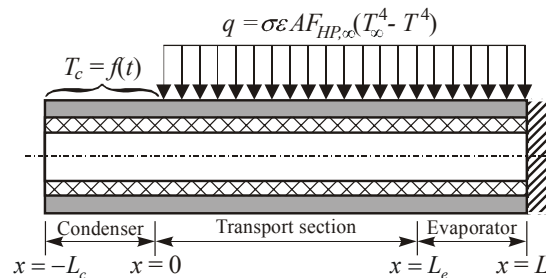


Figure 1. Physical model and coordinate system.

The heat pipe's working fluid initial condition is a supercritical thermodynamic state. Therefore, as the working fluid mass and the void volume of the heat pipe are known, it is possible to determine the specific volume of the working fluid ( $v_{HP}$ ) and, therefore, the initial vapor pressure ( $P_0$ ). When the startup process begins, a temperature gradient develops at  $x = 0$  (see Fig. 1) because the cooling effect resulting from the condenser heat rejection is not propagated throughout the entire heat pipe. Considering the pressure of the working fluid essentially uniform, the axial temperature gradient induces a distribution of working fluid mass inside the heat pipe. As temperature and density are inversely related for a given pressure, the greater the temperature gradient between  $x = 0$  and  $x = L$ , the lower the density and so, the greater is the working fluid mass pushed into the condenser region ( $-L_c < x < 0$ ). Also, the working fluid pressure decreases as the startup process proceeds because the temperature of the entire heat pipe is decreasing.

Depending on the initial condition of the heat pipe, the working fluid at the condenser region may achieve a subcooled condition first than a saturated condition. The current analysis considers two cases for the initial condition: the initial specific volume of the heat pipe is much larger than the critical specific volume of the working fluid ( $v_{HP} \gg v_{crit}$ ), or the specific volume is less or near the critical specific volume ( $v_{HP} < v_{crit}$  or  $v_{HP} \sim v_{crit}$ ).

**Case 1 –  $v_{HP} \gg v_{crit}$ :** The first case can be understood by observing the pressure-specific volume thermodynamic diagram shown in Fig. 2-A. At the beginning of the process the heat pipe is considered to be isothermal at  $T_0$ , where the initial condition of the heat pipe is represented by point 1 in the supercritical region. As the start-up proceeds, a horizontal line of uniform pressure represents the thermodynamic state of the heat pipe. This line lowers as the pressure of the vapor decreases due to the heat rejection at the condenser region. In Figure 2-A, point 2a represents the specific

volume at the condenser end, and point 2b represents the specific volume at the evaporator end (which are at different temperatures due to the temperature gradient existing at  $x = 0$ ). It is important to observe, at the thermodynamic state 2, that the vapor pressure is lower than the critical pressure, but the temperature of the condenser remains above the critical temperature. As the temperature of the condenser continues to decrease, the condenser will enter the superheated region when the temperature of the condenser decreases below the critical temperature, or  $T_c < T_{crit}$ . The condensation process will start when the temperature of the condenser equals the saturation temperature (point 3b) at the vapor pressure at point 3b [ $T_c = T_{sat}(P_v) \equiv P_v = P_{sat}(T_c)$ ]. In this moment, liquid condenses at the wick structure (point 3a), and saturated vapor fills the vapor space at the condenser region (point 3b). The remaining length of the heat pipe remains dry in a superheated condition (line 3b – 3c). As the temperature of the condenser continues to decrease (line 4a – 4c), more liquid condenses in the wick structure, increasing the momentum of the liquid column, which eventually advances towards the evaporator. The process continues until the heat pipe is completely primed, and the thermodynamic state at the wick structure and vapor space is given by points 5a and 5b, respectively.

**Case 2 –  $v_{HP} < v_{crit}$  or  $v_{HP} \sim v_{crit}$ :** The second case can be understood by observing the pressure-specific volume diagram shown in Fig. 2-B and the thermodynamic states schematics shown in Fig. 3. At the beginning of the process the initial condition of the heat pipe is represented by point 1. In this case, as the startup continues, the condenser will reach the critical temperature before the vapor pressure decreases below the critical pressure, at point 2a. At this point, the vapor inside the condenser region changes from supercritical fluid to subcooled liquid because its temperature is below the critical temperature, but the vapor pressure is still greater than the critical pressure ( $T_c < T_{crit}$  and  $P_v > P_{crit}$ ). On the absence of gravitational forces, the subcooled liquid fills the wick structure and the vapor space in the condenser region forming a subcooled liquid slug (Brennan *et al.*, 1993). As the temperature of the condenser decreases, this slug

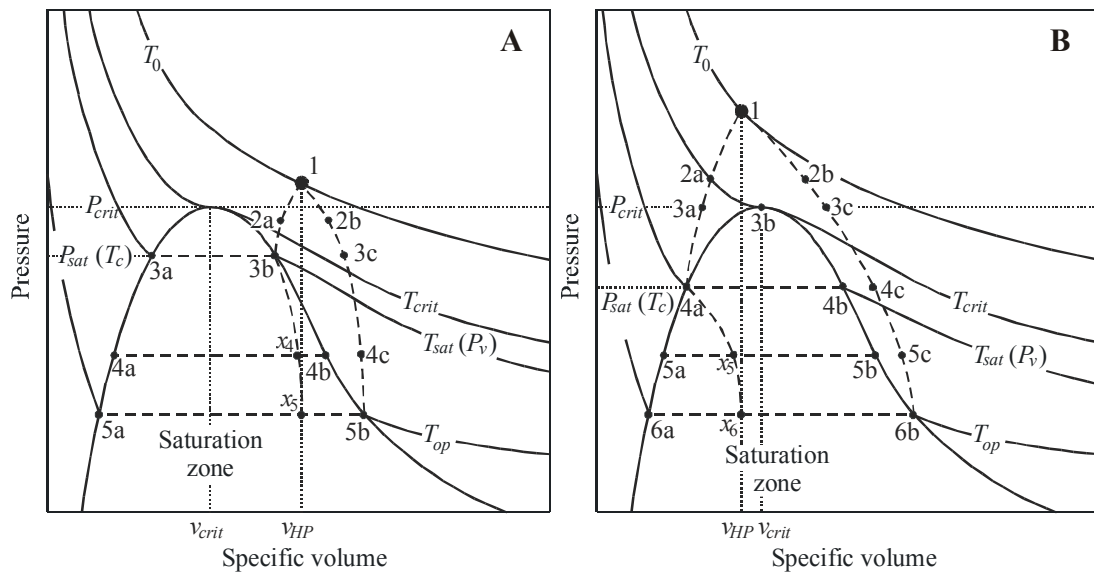


Figure 2. Pressure-specific volume diagram for: (A)  $v_{HP} \gg v_{crit}$  and (B)  $v_{HP} < v_{crit}$ .

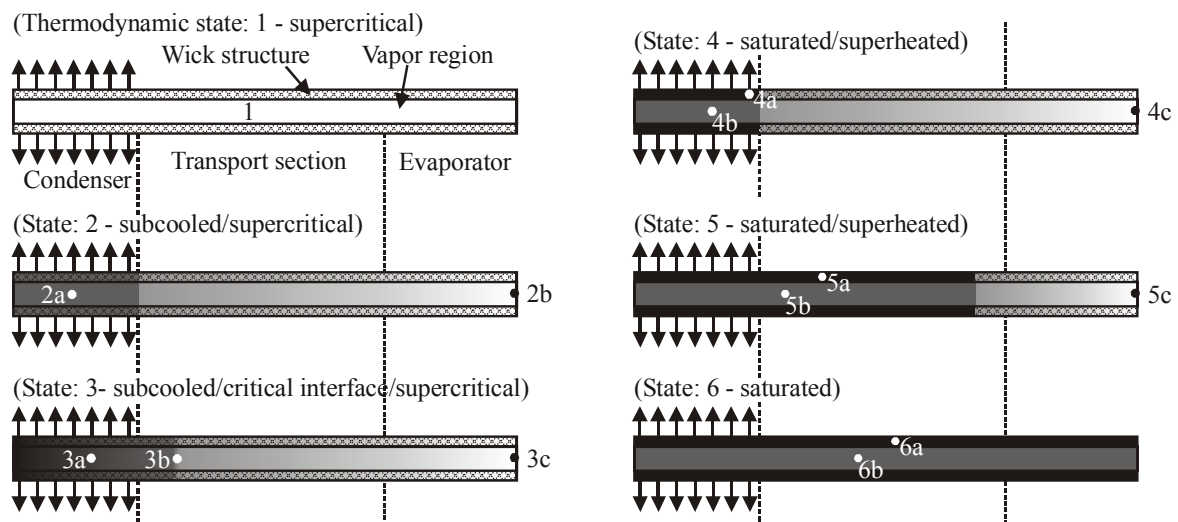


Figure 3. Thermodynamic state schematics for  $v_{HP} < v_{crit}$ .

extends into the transport section until the vapor pressure equals the critical pressure at point 3c. At point 3b, the leading edge of the subcooled slug will be at a critical condition once the local temperature and pressure are equal to the critical temperature and pressure ( $T_{|x=s-L_c} = T_{crit}$  and  $P_v = P_{crit}$ ). From this point on, the length of the subcooled liquid slug decreases until the condenser temperature reaches the saturation pressure at that point in time [ $T_c = T_{sat}(P_v)$ ] at point 4a. At this point, the condenser region is filled with saturated working fluid: saturated liquid at the wick structure (point 4a) and saturated vapor at the vapor space (point 4b). The remaining length of the heat pipe remains dry, in a superheated condition (point 4c). As the temperature of the condenser continues to decrease (line 5a – 5c), more liquid condenses, increasing the momentum of the liquid column, which eventually advances towards the evaporator. The process continues until the heat pipe is completely primed and the thermodynamic state at the wick structure and vapor region is given by points 6a and 6b, respectively.

### 3. Thermal Model

The thermal model used here for the supercritical startup thermodynamic analysis was presented by Couto (2003) and it consists of the following sub-models: conductive for the heat pipe wall, liquid column, and a vapor pressure, all solved for two stages. In the 1<sup>st</sup> stage (see Fig. 1), the heat pipe contains only supercritical vapor and the primary mechanism of heat transfer is axial conduction through the heat pipe's wall. In this case, the conductive model is used to determine the axial temperature profile. When the condensation of working fluid occurs in the condenser region (2<sup>nd</sup> stage), the conductive model and the liquid column model are solved together to determine the axial temperature profile and the liquid column length. The vapor pressure model is iteratively used to determine the working fluid pressure. The vapor pressure and temperature at the condenser region are used as parameters to determine the beginning of the condensation process. The transient, axial temperature distribution in the heat pipe wall is given by:

$$(\rho c)_{eff} \frac{\partial T}{\partial t} = \frac{\partial}{\partial x} \left( k_s \frac{\partial T}{\partial x} \right) + \frac{\sigma \varepsilon A F_{HP,\infty} (T_\infty^4 - T^4)}{V_s}; \text{ for } 0 < x < L \text{ and } t > 0 \quad (1)$$

where  $\alpha_{eff}$  is the effective thermal diffusivity of the heat pipe,  $T$  is the temperature of the heat pipe wall,  $\sigma$  is the Stefan-Boltzmann constant,  $\varepsilon$  is the emissivity of the external wall of the heat pipe,  $A$  is the external area of the heat pipe from  $x = 0$  to  $x = L$ ,  $F_{HP,\infty}$  is the view factor between the heat pipe and the surrounding environment,  $T_\infty$  is the temperature of the surrounding environment,  $k_s$  is the conductivity of the heat pipe wall, and  $V$  is the volume of the heat pipe wall. The second term on the right hand side of Eq. (1) accounts for the radiative parasitic heat load applied over the heat pipe external wall. To account for the heat capacity of the working fluid in the effective thermal diffusivity, a constant coefficient that accounts for the total change of the internal energy from the initial state to the final state for the heat pipe wall and the working fluid was added to the thermal diffusivity of the wall. Details can be found in Couto (2003) and Yan and Ochterbeck (1999). The initial condition for Eq. (1) is assumed as a constant temperature  $T_0$  for the entire heat pipe length. For the 1<sup>st</sup> stage of the model, the boundary conditions at the interface between the condenser and the transport section is a time-variable temperature given by the cryocooler, [ $T_{|x=0} = T_c = f(t)$ ], while the evaporator end is considered adiabatic ( $\partial T / \partial x|_{x=L} = 0$ ). As Eq. (1) is non-linear in temperature due to the parasitic heat load term, a numerical solution based on the finite volume method described by Patankar (1980) was used.

When the vapor pressure inside the heat pipe equals the saturation pressure at a given condenser temperature [ $P_v = P_{sat}(T_c)$ ], the working fluid in the condenser section will achieve a saturation condition, and vapor begins to condense at the wick structure. A liquid column develops inside it, with saturated liquid flowing within the liquid column with an average velocity  $U$ . Once the wick structure is filled with saturated liquid, the liquid column will advance in the direction of the evaporator end with a rewetting velocity  $U_r$ . At the leading edge of the liquid column, liquid is vaporized because the dry region of the heat pipe is at a higher temperature. Also, the parasitic heat load will vaporize some liquid along the column. If the summation of the parasitic heat load and the heat supplied by the dry region is greater than that heat needed to vaporize the entire advancing liquid column, the rewetting process will stagnate. The total length of the liquid column is  $s$ , and its temperature is considered to be uniform and equal to the temperature of the heat pipe wall. At the condenser, this temperature is equal to the cryocooler temperature. Figure 4 shows the physical model for the supercritical startup considering the rewetting process of the liquid column.

The liquid column length is determined from a heat balance at the leading edge of the liquid column [ $x = s(t) - L_c$ ]. The heat balance takes into account the heat conducted from the dry region of the heat pipe and the liquid evaporated at the leading edge of the liquid column.

The liquid column velocity is determined from a lumped momentum balance at the entire liquid column. As the parasitic heat load evaporates liquid along the liquid column length, a mass balance is performed at the liquid column length. These momentum and mass balances provide expressions for the liquid velocity  $U$  as a function of the thermodynamic properties, liquid column length  $s(t)$ , and parasitic heat load  $q_p$ . More details about this derivation can be found in Couto (2003) and Couto *et al.* (2002). The expression for a sintered metal porous wick structure with porosity  $\phi$  and permeability  $K$  is shown below:

$$U = \frac{2\sigma\phi K^{1/2}}{\mu_\ell s} - \frac{q_p'' [2\pi r_w (s - L_c)]}{\rho_\ell A_\ell h_{fg}} \quad (2)$$

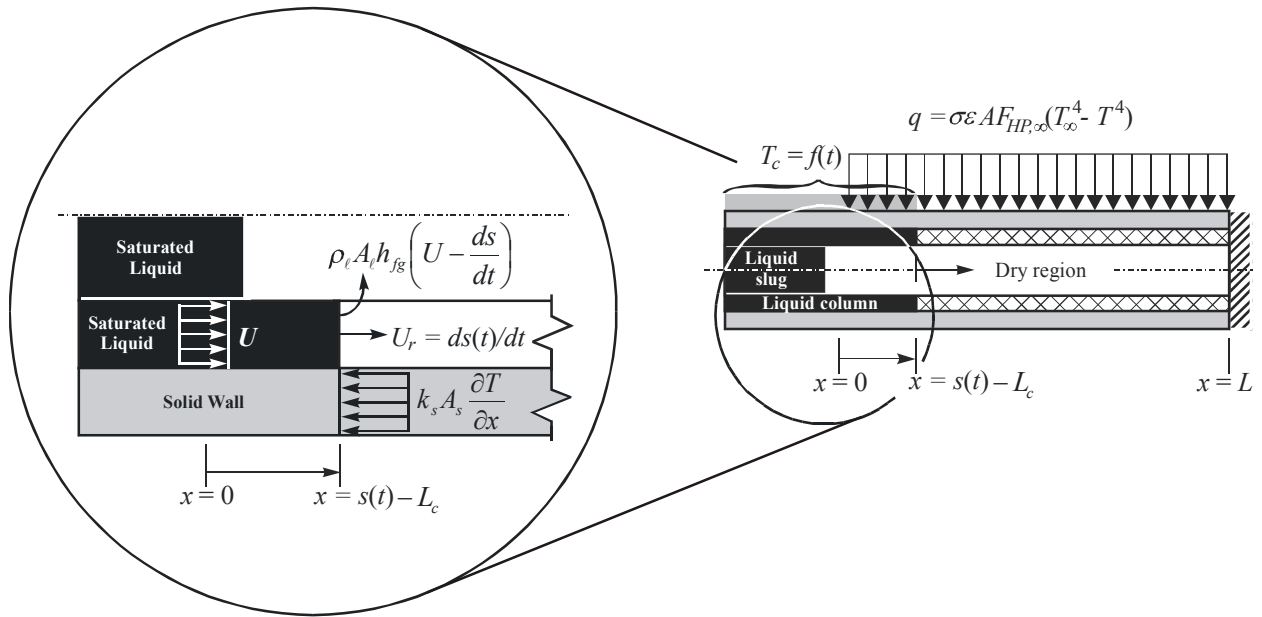


Figure 4. Physical model and coordinate system for the 2<sup>nd</sup> stage of the supercritical startup.

where  $\sigma$  is the surface tension of the saturated liquid,  $\mu_l$  and  $\rho_l$  is the dynamic viscosity and density of the saturated liquid,  $s$  is the liquid column length,  $q_p''$  is the parasitic heat flux,  $r_v$  is the vapor region diameter of the heat pipe,  $L_c$  is the condenser length,  $A_l$  is the liquid filled area of the wick structure, and  $h_{fg}$  is the latent heat of vaporization of the working fluid.

The vapor pressure is modeled according to the real gas thermodynamic equation. Temperature dependant thermodynamic properties are considered for the calculations. The methodology presented by Jacobsen *et al.* (1997) is used to obtain the thermophysical properties of the working fluid. This methodology is based on a fundamental equation, function of the dimensionless Helmholtz energy parameter.

More details about the model can be found in Couto (2003) and Couto *et al.* (2002).

#### 4. Microgravity Startup Analysis

Three sets of microgravity experimental data are used for the thermodynamic analysis in this section: two sets from Brennan *et al.* (1993) and one from Rosenfeld *et al.* (1995). Brennan *et al.* (1993) conducted a microgravity experiment for two different aluminum/oxygen axially grooved heat pipes (TRW heat pipe and Hughes Aircraft Company - HAC heat pipe). Rosenfeld *et al.* (1995) presented an experimental study of the supercritical startup of a titanium/nitrogen heat pipe (NHP).

##### 4.1. Results for the TRW heat pipe

The experiment of the TRW and HAC heat pipes was flown aboard the STS-53 space shuttle mission in December 1992. Reliable startups in flight of the two aluminum/oxygen axially grooved heat pipes were performed, but the startup process in microgravity was slower than that obtained in ground tests. Brennan *et al.* (1993) concluded that in a microgravity environment the condensation of the working fluid develops a liquid slug in the condenser region. In ground tests the excess of liquid spreads in the wick structure due to the effects of the gravitational forces facilitating the startup. In this case, the liquid typically forms a puddle due to the very low surface tension of cryogenic fluids. The TRW heat pipe started successfully after 6 hours at a temperature of 70 K, while the HAC heat pipe started after 6.5 hours at a temperature of 115 K. Brennan estimated the parasitic heat loads of the TRW heat pipe to be from 1.1 W up to 1.9 W at 60 K, while for the HAC heat pipe the parasitic heat load was estimated to be 1.14 W at 119 K.

Figure 5 shows the comparison between the theoretical model and the experimental flight data for the TRW aluminum/oxygen cryogenic heat pipe start-up. The overall agreement between the model and the experimental data is good. Figure 6 shows the pressure-specific volume diagram for the supercritical start-up of the TRW cryogenic heat pipe. The specific volume is shown at the interface between the condenser and transport section ( $x = 0$ ) and for the evaporator end ( $x = L$ ). The circles at the lines represent the thermodynamic state of the heat pipe for each parasitic heat load considered for the calculation. The condensation process will begin at  $T_c = 153.6$  K, from the saturated liquid line. It means that for a short period of time (for less than 2 min), the condensed liquid in the condenser region will be in a sub-cooled condition. After the condensation process begins, the quality at the condenser remains closer to zero until the liquid column starts to move towards the evaporator end. This is because more liquid is being condensed as the temperature of the condenser decreases.

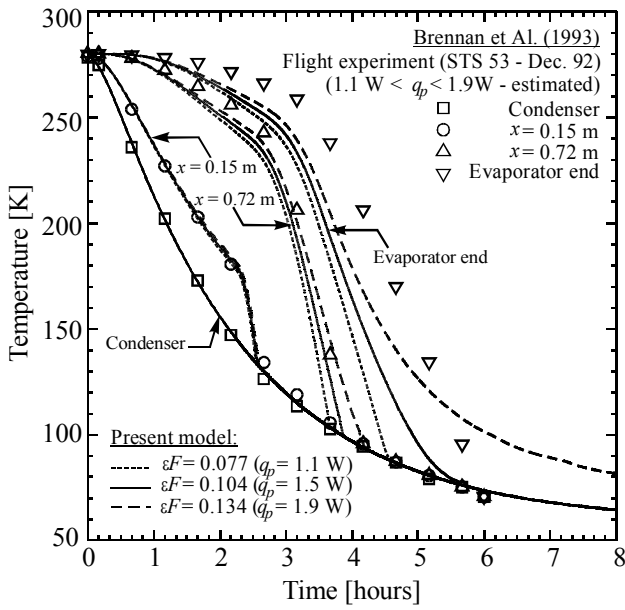


Figure 5. Comparison between the theoretical model and the TRW experimental data.

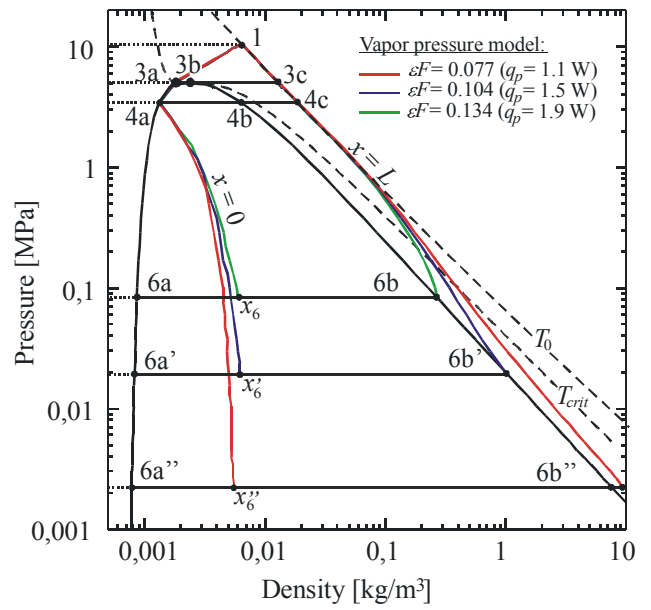


Figure 6. Pressure-specific volume diagram (TRW heat pipe).

The liquid fill rate as a function of the temperature of the condenser is shown in Fig. 7. The liquid fill is defined as the ratio between the condensed liquid mass  $m_\ell$  and the mass that the wick structure can hold  $m_w$ :

$$N = \frac{m_\ell}{m_w} = \frac{(1-x)A_c s / v_c}{A_w s / v_\ell} \quad (3)$$

where  $x$  is the quality of the saturated fluid in the wetted region,  $A_c$  is the cross sectional area of the condenser (liquid + vapor),  $s$  is the position of the liquid column for a given time,  $A_w$  is the cross sectional area of the grooves, and  $v_c$  and  $v_\ell$  are the specific volumes of the saturated fluid in the wetted region and saturated liquid, respectively. If  $N = 1$ , the mass of liquid is enough to fill the grooves with no excess liquid. For  $N > 1$  there is excess liquid. It can be observed that there is a large excess of liquid when the start-up process begins. This is because the oxygen enters the saturation zone from a sub-cooled condition. Therefore, the condenser is flooded with saturated liquid. The fill rate starts to decrease as the liquid column advances, and as the liquid specific volume decreases with continued decrease in temperature.

Figure 8 shows the position of the liquid column ( $s$ ) inside the axial grooves as a function of time. Also the position of the liquid slug is shown. The slug was observed by Brennan *et al.* (1993) and it only occurs in microgravity environment. On the ground, the capillary forces cannot support a slug across the vapor region, and excess of liquid is

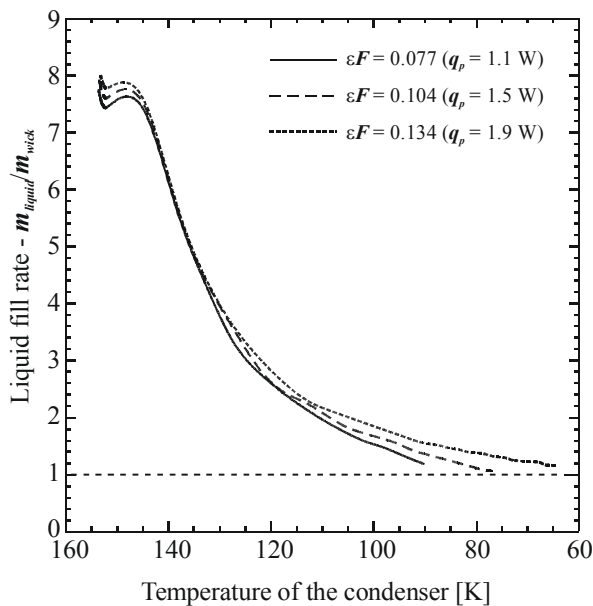


Figure 7. Liquid fill rate (TRW heat pipe).

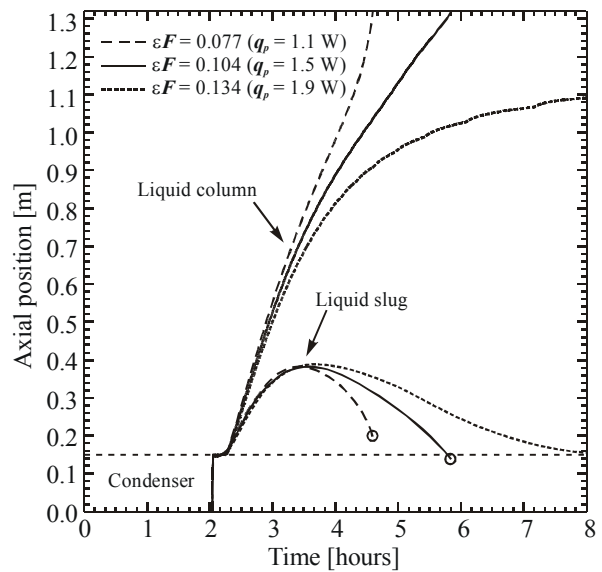


Figure 8. Predicted liquid slug and liquid front position (TRW heat pipe).

spread as a puddle. This effect facilitated the priming of a heat pipe in ground tests. As shown in Fig. 8, when the start-up process begins, the liquid column remains stagnated at the interface between the condenser and the transport region for a few minutes (12.5 min.). This is because the liquid velocity in the liquid column is not sufficient to provide the cooling to the dry region of the heat pipe. As the temperature of the condenser decreases, the surface tension of the working fluid increases, thus, increasing the capillary driving force, causing the liquid velocity to increase. So, the liquid column will eventually advance towards the evaporator end. For a lower parasitic heat load (1.1 W), the start-up process was faster, because less fluid was evaporated from the liquid column. For a higher parasitic heat load (1.9 W), the analytical model shows that the heat pipe would not prime completely, with the liquid column stagnating at about 0.21 m from the evaporator end.

The position of the slug was determined from the data shown in Fig. 7, for  $N > 1$ . The position of the liquid slug increases with time until it reaches a maximum at about 0.40 m from the condenser end, and then it decreases. For the lowest parasitic heat load (1.1 W) the position of the slug when the heat pipe primed is at 0.20 m from the condenser end. This is because the mass of 10.3 g of oxygen on the TRW heat pipe was designed to fill the wick structure with saturated liquid and no excess at 60 K, but the heat pipe was completely primed at 90 K. The data presented in Fig. 7 shows that there is an excess of liquid of 1.8 g at 90 K, while the mass of liquid inside the wick structure is 8.1 g. The remaining 0.4 g is the mass of saturated vapor. For the average parasitic heat load of 1.5 W, the heat pipe primed at about 75 K, and the slug was at 0.14 m from the condenser end. It is important to say that if the temperature of the heat pipe continues to decrease until 60 K, there will be no liquid excess, and therefore, no slug. For the highest parasitic heat load, the liquid slug was stagnated at 0.15 m, as the heat pipe did not prime completely.

## 4.2. Results for the HAC heat pipe

Figure 9 shows the comparison between the theoretical model and the experimental data for the HAC (Hughes Aircraft Co.) aluminum/oxygen cryogenic heat pipe start-up. The comparison is considerably good for the heat conduction model (1<sup>st</sup> stage of the startup process). The condensation of the working fluid started at a temperature far below the oxygen critical temperature (154.6 K), around 128 K. This is because the vapor pressure only drops below the critical pressure when the condenser temperature drops below 128 K. This phenomenon is better observed by analyzing Figure 10, which presents a pressure-specific volume diagram for the supercritical startup of the oxygen/aluminum HAC heat pipe. The supercritical startup process of the HAC heat pipe starts at 285 K, at a pressure around 20 MPa (point 1 in Figure 10<sup>1</sup>). As the condenser cools down, the vapor pressure decreases. When the condenser cools to a temperature equal to the oxygen critical temperature ( $T_{crit} = 154.6$  K) at point 2a, the pressure of the working fluid inside the heat pipe is still greater than the oxygen critical pressure ( $P_2 = 8953$  kPa  $>$   $P_{crit} = 5043$  kPa). As the condenser continues to cool down, a subcooled liquid slug is formed in the condenser region of the heat pipe. When the pressure of the working fluid equals the oxygen critical pressure, the temperature at the condenser end is 128 K (point 3a). At this point in time, the subcooled liquid slug extended for 0.17 m in the adiabatic section of the HAC heat pipe (point 3b). As the startup process continues, the subcooled liquid slug recedes until the condenser is completely filled with saturated working fluid at a temperature of 122 K. At this point, the working fluid pressure equals the saturation pressure at 122 K, and the rewetting process starts. The thermodynamic condition of the saturated liquid in the wick structure is given

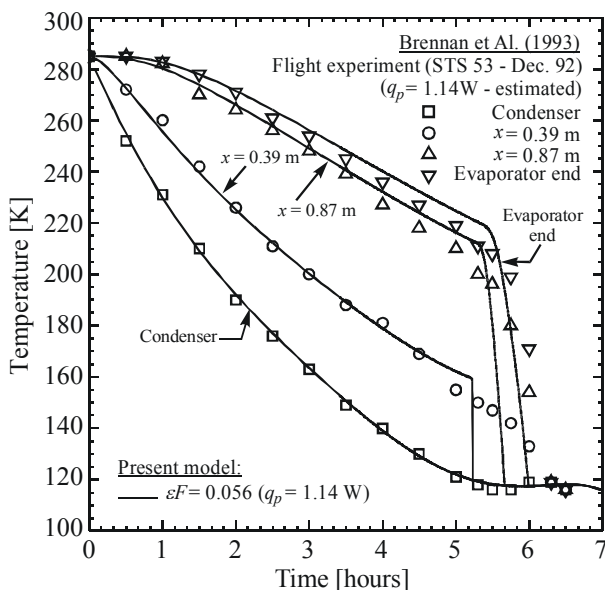


Figure 9. Comparison between the theoretical model and the HAC experimental data.

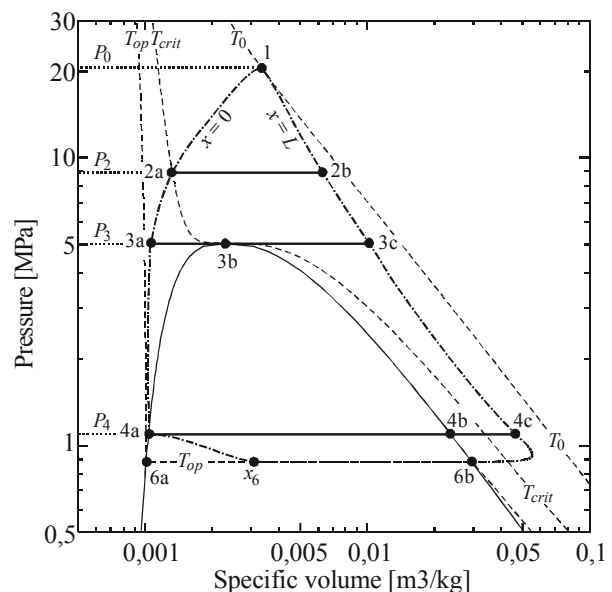


Figure 10. Pressure-specific volume diagram (HAC heat pipe).

<sup>1</sup> The number of the points in this figure agree with those in Figure 2-B

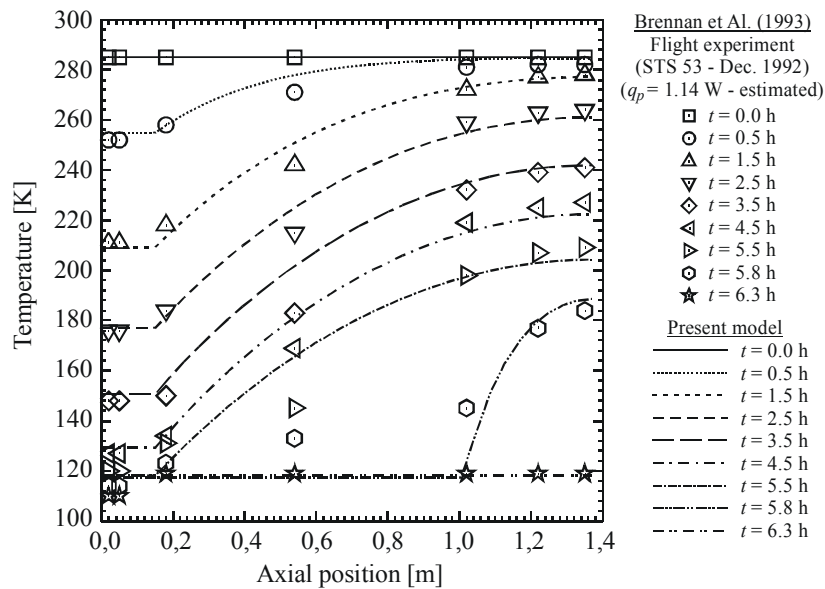


Figure 11. Temperature vs. axial position at different times (HAC heat pipe).

by point 4a and the saturated vapor in the vapor region, by point 4b. The remaining length of the heat pipe (line 4b – 4c) is at a superheated condition. According to Figure 10 the theoretical rewetting process is faster than the experimental process presented by Brennan *et al.* (1993). This is because at 120 K the capillary force developed at the grooves of the HAC heat pipe are large enough to accelerate the saturated liquid column towards the evaporator end. As the liquid column starts to advance, more vapor is condensed, decreasing the specific volume of the superheated vapor at the evaporator end as shown by the line that connect points 4c and 6b in Figure 10. The heat pipe reached an operational steady state at 117.5 K after 6 hours of the beginning of the startup process.

Figure 11 shows the comparison of theoretical and experimental axial temperature profiles for different times. The overall comparison is good and the trends of the model agree with the physics of the process.

### 4.3. Results for the NHP heat pipe

Rosenfeld *et al.* (1995) presented a study of the supercritical startup of a titanium/nitrogen heat pipe (NHP). The test was performed during mission STS-62 (March 1994). This heat pipe reached a non-operational steady state thermal condition during microgravity tests. Only 30 % of the heat pipe length cooled below the nitrogen critical point temperature, but the vapor pressure was still above the critical pressure (the vapor pressure was estimated based on the experimental temperature data). However, Rosenfeld *et al.* (1995) observed that in ground tests, the titanium/nitrogen heat pipe underwent startup successfully. The authors concluded that, with the addition of parasitic heat loads, the thermal conduction of the titanium/nitrogen heat pipe was insufficient to allow for the internal pressure to decrease below the critical pressure of nitrogen when in microgravity. From the point of view of these authors “(...) if the heat pipe could not be cooled sufficiently by radiation or conduction to allow the internal pressure to reach the critical pressure, then a non-operational steady state will be achieved”. The successful startup during ground tests was due to enhanced thermal transport of the gravity-assisted convection/liquid collection effects.

Although little information regarding the parasitic heat load and the geometry of the wick structure of this heat pipe is available at Rosenfeld *et al.* (1995), the experimental data for this unsuccessful startup can be used for comparison with the presented model, and some conclusions can be drawn regarding the titanium/nitrogen heat pipe. The wick structure of the NHP was composed by six porous copper cables with a circular section of 3.2 mm of diameter held against the internal diameter of the titanium alloy (Ti-6 Al-4V ELI) pipe by a full-length centered spring. The authors did not present values for the porosity and permeability, but typical values can be found in the literature (Faghri, 1995):  $0.520 \leq \phi \leq 0.895$  (porosity);  $0.009 \text{ m}^2 \leq K \leq 12.4 \text{ m}^2$  (permeability  $\times 10^{-10}$ ). According to Eq. (2) which gives an average velocity of the saturated liquid in a porous wick structure, the combination of  $\phi$  and  $K$  that produces the largest velocity are  $\phi = 0.895$  and  $K = 12.4 \times 10^{-10} \text{ m}^2$ . Also, the largest porosity provides more void volume in the wick structure to be filled with liquid, and therefore, it provides a lower vapor pressure during startup if compared to a lower porosity. Therefore, two theoretical cases were considered for comparison - case 1:  $\phi = 0.895$  and  $K = 12.4 \times 10^{-10} \text{ m}^2$ ; and case 2:  $\phi = 0.520$  and  $K = 0.009 \times 10^{-10} \text{ m}^2$ .

Figure 12 present the comparison between the experimental data of Rosenfeld *et al.* (1995) and the theoretical model. The comparison is good and the model predicted the unsuccessful startup of the titanium/nitrogen heat pipe. This failure is due to the fact that the vapor pressure never reached the critical pressure of the nitrogen in none of the cases, even though the temperature of the condenser was far below the critical temperature of the nitrogen even after 8 hours of testing. The pressure-specific volume diagram for the NHP is shown in Figure 13 for both cases. It can be

observed that, for the largest porosity (case 1), the vapor pressure at steady state reached 6.1 MPa while for the lower porosity the pressure at steady state was 13.3 MPa (more than twice larger!). However, in both cases, the steady state pressure was still higher than the critical pressure of the nitrogen (3.4 MPa), and therefore, no condensation of the working fluid occurred during the startup because a saturation thermodynamic condition was never reached in the titanium/nitrogen heat pipe. The shaded zone in Figure 13 represent any steady state possible for the combination of porosity and permeability within the typical ranges for porous metal wick structures.

Figure 14 shows the comparison between the theoretical axial temperature profile for case 1 and the experimental data presented by Rosenfeld *et al.* (1995). Some overestimations of temperatures are observed, and this can be due to little information about the thermophysical properties of the titanium alloy used in the NHP. Typical values for pure titanium were used for the calculations. Nevertheless, the overall comparison is good.

Concluding, the non-operational steady state reached by the titanium/nitrogen heat pipe was due to a combination of the effects of the parasitic heat loads, low conductance of the titanium wall, and mass of working fluid. The designed working fluid mass of 24.1g provided a high initial pressure, and the low conductance of the heat pipe wall, added to the parasitic heat load, did not provide enough cooling for the vapor pressure to decrease below the critical pressure of the nitrogen. These tests highlighted the significance of the parasitic heat loads, as the heat pipe start-up failure would not occur in microgravity if the heat leaks had been significantly reduced.

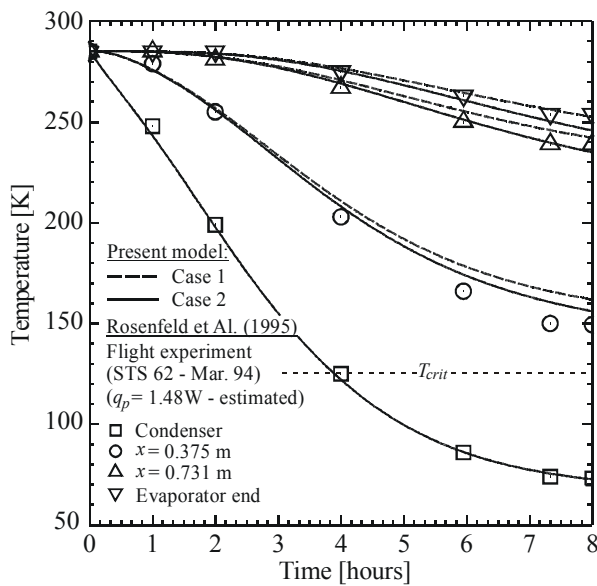


Figure 12. Comparison between the theoretical model and the NHP experimental data.

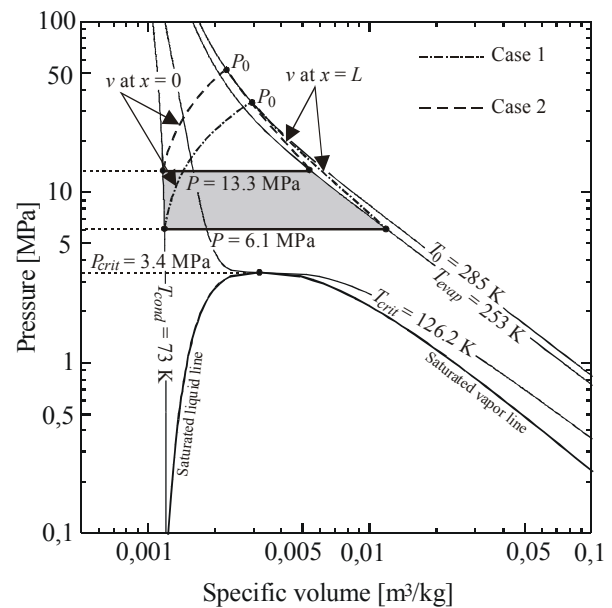


Figure 13. Pressure-specific volume diagram (NHP heat pipe).

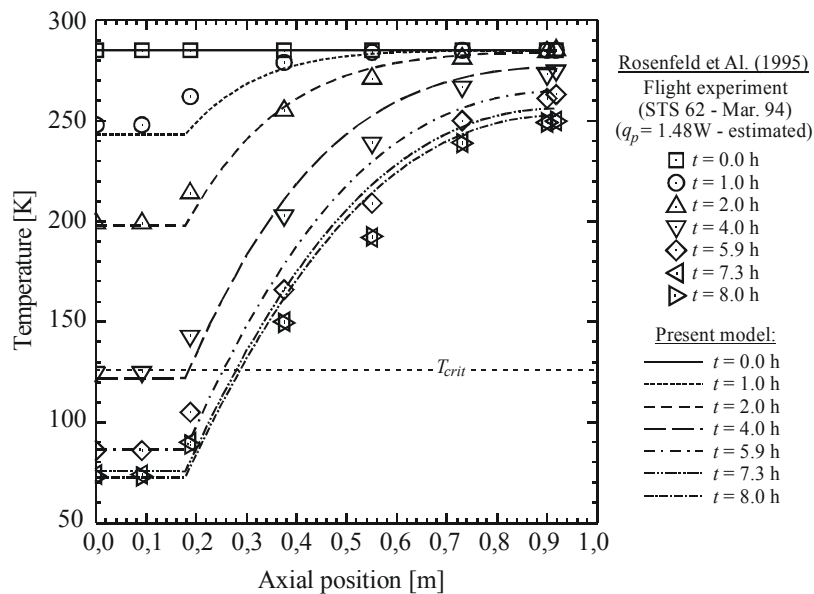


Figure 14. Temperature vs. axial position at different times (NHP heat pipe – case 1).

## 5. Conclusions

The thermodynamic analysis of the supercritical startup of cryogenic heat pipes in microgravity environment provided a good insight of the startup phenomena.

Cryogenic heat pipes are very sensitive to parasitic heat loads. The average condensed liquid velocity drives the rewetting process and it is controlled by the conducted heat flux from the dry region of the heat pipe. The parasitic heat loads increase the temperature gradient in the dry region, increasing the vaporization of fluid at the leading edge of the liquid column. Also, parasitic heat loads vaporize the fluid along the liquid column edge, decreasing the average liquid velocity. These two effects combined decrease the liquid column momentum, and the rewetting process may stagnate before the heat pipe is fully primed for relatively large parasitic heat loads. Additionally, parasitic heat loads may add loads to the heat pipe on the order of the maximum transport capability.

As cryogenic working fluids usually exhibits very low values of surface tension and latent heat of vaporization, resulting in low heat transport capacity heat pipes, even a small amount of parasitic heat load is able to vaporize cryogenic working fluids. A deficiency of working fluid will decrease the vapor pressure during startup, but total amount of working fluid may not be enough to prime completely the heat pipe. An excess of fluid charge will cause an increase of the vapor pressure of the heat pipe. Depending on the combination of parasitic heat loads and excess of fluid charge, the vapor pressure may never decrease below the critical pressure of the working fluid, even if the condenser is at a temperature below the critical point.

## 6. References

- Abrosimov, A., Baryshev, O., Horonenko, V., and Kosorotov, M., 1992, "Diode Cryogenic Heat Pipe for SODART Telescope Silicon Detector Cooling". Proc. of the 8<sup>th</sup> Int. Heat Pipe Conf., Beijing, China, pp. E-P54/1 – E-P54/4.
- Agência especial Brasileira, 1996, "Plano Nacional de Atividades Espaciais – PNAE". Brasilia DF, Brazil.
- Brandt, O. and Schlitt, R., 1997, "Low Temperature Radiator Design for the Abrixas X-Ray Satellite". 6<sup>th</sup> European Symp. on Space Environmental Control Systems, Noordwijk, The Netherlands. Report ESA SP-400, pp. 151 – 159.
- Brennan, P. J., Thienen, L., Swanson, T. and Morgan, M., 1993, "Flight Data for the Cryogenic Heat Pipes (CRYOHP) Experiment". 28<sup>th</sup> AIAA Thermophysics Conference, Orlando, FL, AIAA Paper No. 93-2735.
- Couto, P., 2003, "Theoretical and Experimental Analysis of Supercritical Startup of Cryogenic Heat Pipes". Thesis (Dr.Eng.), Mech. Engineering Dept., Fed. Univ. of Santa Catarina, Florianópolis, Brazil.
- Couto, P., Ochterbeck, J. M. and Mantelli, M. B. H., 2002, "Analysis of Supercritical Start-up Limitations for Cryogenic Heat Pipes with Parasitic Heat Loads". 8<sup>th</sup> AIAA/ASME Joint Thermophysics and Heat Transfer Conf., St. Louis. AIAA Paper No. 2002-3095.
- Faghri, A., 1995, "Heat Pipe Science and Technology". 1<sup>st</sup> Edition, Washington DC: Taylor and Francis.
- Groll, M., Röster, S. and Supper, W., 1986, "Experimental Investigation of a Cryogenic Methane Heat Pipe Diode". Proc. of the 16<sup>th</sup> Intersociety Conf. on Environmental Systems, San Diego, CA, pp. 341 – 348.
- Hamilton, A. and Hu, J., 1993, "An Electronic Cryoprobe for Cryosurgery Using Heat Pipes and Thermoelectric Coolers - A Preliminary Report". Journal of Medical Engineering and Technology, Vol. 17, No. 3, pp. 104 – 109.
- Ishigohka, T., Hirayama, Y., Ninomiya, A. and S. Maezawa., 1999, "Conduction Cooling of High-TC Superconducting Magnet Using Heat Pipe". Proc. of the 11<sup>th</sup> Int. Heat Pipe Conf., Tokyo, Japan, pp. 139 – 144.
- Jacobsen, R. T., Penoncello, S. G. and Lemmon, E. W., 1997, "Thermodynamic Properties of Cryogenic Fluids", 1<sup>st</sup> Edition, New York, NY: Plenum Press.
- Nakano, A., Shiraishi, M., Nishio, M. and Murakami, M., 1998, "An Experimental Study of Heat Transfer Characteristics of a Two-phase Nitrogen Thermosyphon Over a Large Dynamic Range Operation". Cryogenics, Vol. 38, No. 12, pp. 1259 – 1266.
- Ochterbeck, J. M., Peterson, G. P. and Ungar, E. K., 1995, "Depriming/Rewetting of Arterial Heat Pipes: Comparison with Share-II Flight Experiment". AIAA Journal of Thermophysics and Heat Transfer, Vol. 9, No. 1, pp. 101 – 108.
- Patankar, S. V., 1980, "Numerical Heat transfer and Fluid Flow", Washington DC: Hemisphere Pub. Corp.
- Peterson, G. P., 1991, "An Introduction to Heat Pipes – Modeling, Testing and Applications". 1<sup>st</sup> Edition, New York, NY: John Wiley and Sons, Inc.
- Peterson, G. P. and Compagna, G. L., 1987, "Review of Cryogenic Heat Pipes". AIAA J. of Spacecraft, Vol. 24, No. 2.
- Rosenfeld, J. H., Buchko, M. T. and Brennan, P. J., 1995, "A Supercritical Start-Up Limit to Cryogenic Heat Pipes in Microgravity". Proc. of the 9<sup>th</sup> Int. Heat Pipe Conf., Albuquerque, NM, Vol. 2, pp. 742 – 753.
- Röster, S., Groll, M., Supper, W. and Konev, S., 1987, "Analysis and Experimental Investigation of a Cryogenic Methane Heat Pipe". Proc. of the 6<sup>th</sup> Int. Heat Pipe Conf., Grenoble, France, pp. 352 – 355.
- Voyer, E., Moschetti, B., Briet, R., Alet, I. and Evin, R., 1997, "Heat Pipes for Cryogenic Applications on Satellites". 27<sup>th</sup> Int. Conf. on Environmental Systems, Lake Tahoe, Nevada, SAE Technical Paper No. 972450.
- Wright, J. P., 1980, "Development of a 5 W 70 K Passive Radiator". 15<sup>th</sup> AIAA Thermophysics Conf., Snowmass, Colorado, AIAA Paper No. 80-1512.
- Wright, J. P. and Pence, W. R., 1973, "Development of a Cryogenic Heat Pipe Radiator for a Detector Cooling System", SAE-ASME-AIAA-ASMA-AIChE Intersociety Conf. on Environmental Systems, San Diego, California.
- Yan, Y. H. and Ochterbeck, J. M., 1999, "Analysis of Supercritical Start-Up Behavior for Cryogenic Heat Pipes", AIAA Journal of Thermophysics and Heat Transfer, Vol. 13, No. 1, pp. 140 – 145.